Environmental Science & Technology

Article

pubs.acs.org/est

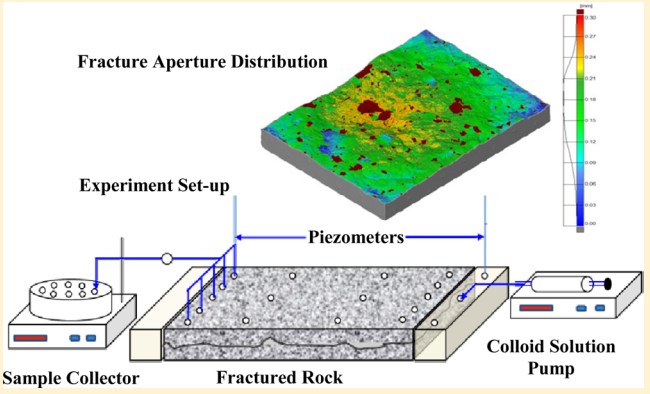
Colloid Transport in Dolomite Rock Fractures: Effects of Fracture Characteristics, Specific Discharge, and Ionic Strength

Pulin K. Mondal[†] and Brent E. Sleep[†,*]

[†]Department of Civil Engineering, University of Toronto, 35 St. George Street, Toronto, Ontario, Canada M5S 1A4

Supporting Information

ABSTRACT: The effects of fracture characteristics, specific discharge, and ionic strength on microsphere transport in variable-aperture dolomite rock fractures were studied in a laboratory-scale system. Fractures with different aperture distributions and mineral compositions were artificially created in two dolomite rock blocks. Transport tests were conducted with bromide and carboxylate-modified latex microspheres (20, 200, and 500 nm diameter). Under overall unfavorable attachment conditions, there was significant retention of the 20 nm microsphere and minimal retention of the 500 nm microsphere for all conditions examined. Aperture variability produced significant spatial variation in colloid transport. Flushing with low ionic strength solution (1 mM) following microsphere transport at 12 mM ionic strength solution produced a spike in effluent microsphere concentrations, consistent with retention of colloids in secondary energy minima. Surface roughness and charge heterogeneity effects may have also contributed to the effect of microsphere size on retention. Matrix diffusion influenced bromide transport but was not a dominant factor in transport for any microsphere size. Calibrated one-dimensional, two-site kinetic model parameters for colloid transport in fractured dolomite were sensitive to the physical and chemical properties of both the fractured dolomite and the colloids, indicating the need for mechanistic modeling for accurate prediction.



INTRODUCTION

Colloid transport in fractured rock systems is relevant to pathogen (e.g., viruses, bacteria) transport and colloid facilitated contaminant transport (e.g., radionuclides sorbed on natural colloid) in fractured aquifers, and delivery of remediation agents (e.g., engineered bacteria, nano zerovalent iron particles) to contaminated fracture zones. Colloid transport in fractures has been investigated through numerical investigations,[1−3] field scale tests in crystalline bedrock,[4−6] and fractured clay-rich till,[7] and lab-scale tests with fractured shale saprolite core[8,9] and fractured tuff.[3,10] These studies indicated that the physicochemical nature of the fractured rock−groundwater−colloid system strongly affects the fate of colloids.

The transport of colloids in a fracture can be enhanced due to flow channeling and size exclusion of larger colloids from small aperture regions.[1,2,11] Abdel-Salam and Chrysikopoulos[1] and James and Chrysikopoulos[2] showed with numerical studies that increased fracture aperture variability leads to faster transport and increased dispersion of colloid (1 μm in size). Colloid transport in fractured rock can be retarded due to hydrodynamic dispersion and matrix diffusion. Bales et al.[10] suggested that diffusion of colloid (bacteriophage) into shallow pores of the matrix in fractured tuff could be responsible for the apparent retardation of the colloid. However, McKay et al.[12] in field experiments with bacteriophages (MS2 and PRD1) in fractured clay-rich till found that these colloids mainly traveled through fractures with minimal diffusion into the porous matrix.

Attenuation of colloid transport in fractured rock may also be dependent on solution chemistry, and surface charge of the fractured rock minerals and the colloids. Dissimilar surface charges of the minerals and colloids provide a favorable condition for attachment, and significant colloid retention in the fracture is expected. In contrast, under unfavorable attachment conditions, colloids can still be attached to the minerals due to the presence of secondary energy minima (a weaker attractive energy well in the Derjaguin−Landau−Verwey−Overbeek (DLVO) interaction energy profile)[13,14] or to patches of oppositely charged sites associated with commonly occurring surface charge heterogeneity.[15,16]

Fractured carbonate-rock (limestone and dolomite) aquifers are often used for both community and noncommunity water supplies; and may be at risk of pathogen contamination from various sources (e.g., onsite septic systems, manure fields). Improving the understanding of the mechanisms of colloid

Received: May 3, 2012
Revised: August 8, 2012
Accepted: August 14, 2012
Published: August 14, 2012

Downloaded via SANDIA NATL LABORATORIES on January 13, 2026 at 20:14:22 (UTC).
See https://pubs.acs.org/sharingguidelines for options on how to legitimately share published articles.

 © 2012 American Chemical Society

transport in fractured dolomite and limestone, particularly with virus and virus-sized colloids, is important for developing policies and practices to protect the safety of water supplies in fractured rock aquifers. At present, the factors controlling virus and virus-sized colloid transport in discrete fractured carbonate rocks have not been fully explored, although there have been studies on the transport of biocolliod at the bench scale[17] and the field scale.[18] The objectives of this study are to quantify, at the lab scale, the effects of the physical and chemical characteristics of dolomite rock, specific discharge, and ionic strength on the transport of virus-sized and microbacteria-sized microspheres. Two dolomite fractures with different physical and chemical characteristics were artificially created in two dolomite rock blocks. The fractures were characterized for fracture geometry and mineralogy. Transport tests in the fractures were performed with a conservative solute (bromide) and three carboxylate-modified latex microspheres at three specific discharges and two ionic strengths.

MATERIALS AND METHODS

Rock Fracture and Characteristics. In each of two dolomite rock (from a quarry in Wiarton, Ontario, Canada) blocks (280 × 210 × 70 mm in size) a single fracture was created along stylolites following the procedure described by Reitsma.[19] The fractures were characterized for surface roughness and aperture distribution using a 3D stereo-topometric measurement system, the ATOS II (GOM mbH, Germany). These fractures will be referred to as Fracture F1 and Fracture F2. The aperture fields of these fractures generated by ATOS II were used to determine the statistics of the aperture distribution using Origin 8.5. Waste rock materials generated during the fracture preparation were used to determine the matrix porosity, mineral composition, and surface charge. The matrix porosity was determined using scanning electron microscope-backscatter electron (SEM-BSE) image analysis on epoxy-impregnated polished rock samples. The mineral composition was determined with X-ray diffraction (XRD) and X-ray fluorescence spectroscopy (XRF). Surface charges of the crushed rock materials were measured by SurPASS Electrokinetic Analyzer (Anton Paar GmbH) at different solution conditions. Hydraulic tests to determine the equivalent hydraulic aperture were also performed. There were five collection ports near the downstream side of the fractures. The methods are outlined in detail in the Supporting Information.

Solutions. The solutions used in the hydraulic and tracer transport tests were prepared with distilled, degassed Milli-Q water. The water was buffered with 1 mM sodium bicarbonate ($NaHCO_3$) to buffer the water pH ≈ 8.2, and sodium chloride (NaCl) solution was added to the buffered water at the concentrations of 1 mM and 10 mM. Sodium bromide (NaBr) solution was added to the solutions at a concentration of 1 mM to prepare the tracer solutions. The total ionic strengths (IS) of the solutions were 3 and 12 mM, and the measured electrical conductivities were 328 ± 7 and 1378 ± 38 $\mu S.cm^{-1}$, respectively. The background solutions were prepared similarly, except 1 mM NaBr was replaced with 1 mM NaCl. The average temperature of the tracer and background solutions was 21.0 ± 0.3 °C, and the average pH of all of these solutions was 8.2 ± 0.3.

Microsphere Characteristics. Carboxylate-modified latex (CML) fluorescent microspheres of 20, 200, and 500 nm (from Molecular Probes, Invitrogen Canada Inc.) were used in the transport tests. The solutions containing microspheres were prepared with buffered and ionic strength (IS) adjusted distilled Milli-Q water to provide final microsphere concentrations of 4.55×10^{11}, 6.37×10^{8}, and 4.66×10^{7} Particles·mL^{-1} ($P_t \cdot mL^{-1}$) for 20 nm (M-1), 200 nm (M-2), and 500 nm (M-3) microspheres, respectively. Microspheres in the prepared solution and samples from transport tests were analyzed by using a fluorescence spectrophotometer. Zeta potentials and hydrodynamic diameters of the microspheres were measured at different solution conditions using the dynamic light scattering technique with a Zetasizer Nano ZS (Malvern Instruments). Description of the microspheres and these methods are provided in the Supporting Information.

Transport Tests. The transport tests were conducted in a fractured rock specimen that was placed in a steel cell with the sides and an inlet chamber sealed. Five outlet ports near the downstream end of the fracture were combined to form an outlet manifold, and it was connected to a fraction collector for outlet samples collection. A syringe pump was used to inject tracer and background solutions, and glass tube piezometers at the inlet chamber and outlet manifold were used for water head measurement. A schematic of the experimental setup is provided in the Supporting Information. In the transport test, the solution containing microspheres was injected into the fractures as a pulse of 11 pore volumes (PV, calculated based on the equivalent hydraulic aperture of the fractures) followed by injection of 18 PV of buffered solution with no bromide and microspheres. For both fractures, the tests were conducted at three specific discharges of 0.35, 0.7, and 1.05 mm·s^{-1}. Some transport tests were performed at the specific discharge of 1.05 mm·s^{-1} keeping the five outlet ports at the outlet manifold separate. Bromide (∼ 80 mg·L^{-1}) was used in all transport tests as a conservative solute tracer. For Fracture F1, three sets of colloid transport tests at 3 mM ionic strength (IS) were conducted with the fractures before the tests reported in this work. Between the first and second tests, decreases in retention of the smallest microspheres were observed, indicating irreversible saturation of some attachment sites. For Fracture F2, six tests at various IS were performed before the tests reported in this work.

Modeling Solute and Colloid Transport. The breakthrough curves (BTCs) of the bromide and microspheres were modeled using HYDRUS-1D,[20] a one-dimensional advection-dispersion transport model accounting for the nonequilibrium processes. A two-region model with dual-porosity type transport process (a physical nonequilibrium model) was used to model the bromide BTCs. The physical nonequilibrium model alone was not adequate to fit the microsphere BTCs. The microsphere transport in this study was modeled using chemical nonequilibrium (two-site kinetic) model. For the two-site kinetic model, the model has two attachment coefficients (K_{att1} and K_{att2}) and two detachment coefficients (K_{det1} and K_{det2}) which can be determined by parameter estimation.

RESULTS AND DISCUSSION

Fractured Rock Characteristics. The arithmetic mean and geometric mean of the aperture distribution of Fracture F1 were 196 and 165 μm, respectively. The corresponding values for Fracture F2 were 95 and 88 μm. The kurtosis of the aperture distribution was 32.9 for Fracture F1 and 170.2 for Fracture F2, indicating lower variability in aperture for F2. The skewness of the aperture distribution was 5.24 and 8.48 for Fractures F1 and F2, respectively, indicating presence of a wide

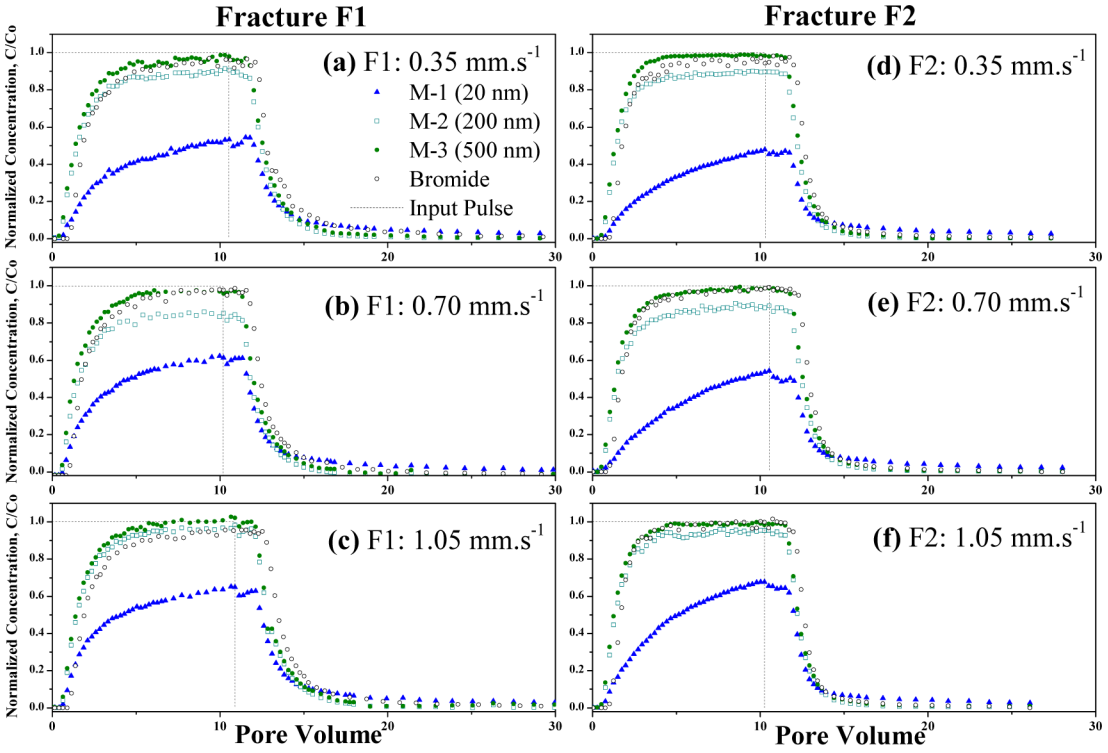


Figure 1. Microsphere BTCs at different specific discharges at Fractures F1 and F2 (ionic strength = 3 mM).

range of aperture value above the mean aperture values. The maximum and minimum roughness values (roughness as defined by Grasselli et al.[21]) of the bottom wall surface of Fracture F1 were 9.84 and 8.73, respectively (average roughness of 9.36). The corresponding roughness values for Fracture F2 were 9.18 and 8.56, respectively (average roughness of 8.89).

In the XRD and XRF analyses of the rock materials, dolomite was the major mineral phase in the bulk rock materials of both fractures (~ 94.9% in Fracture F1 rock materials, and ~96.5% in Fracture F2 rock materials). The minor phases were quartz and potassium-feldspar (<5.1%) in Fracture F1 rock materials, and silica and orthoclase (<4%) in Fracture F2 rock materials. The image analysis, performed on the SEM-BSE images of epoxy-impregnated polished rock samples, provided the porosity of the stylolite areas of ~22 and 13.5% in the rock materials of Fractures F1 and F2, respectively.

At the water pH of 8.2 ± 0.3, the major mineral (dolomite) and minor minerals (quartz, k-feldspar, silica, and orthoclase) of the rock materials are expected to have negative ζ potential (ZP) values as their iso-electric point (IEP) values are lower than pH value of 8.2 (dolomite ~6 to 7, quartz and silica ~3 to 5, k-feldspar ~2 to 3.7, orthoclase ~2 to 2.4).[22−24] The ZP results showed that the rock materials of both fractures were negatively charged for all experimental conditions. The ZP decreased (less negative) with increased ionic strength for both rock materials. For Fracture F1 rock, the ZPs were −39 and −36 mV in 3 mM and 12 mM solutions, respectively. For Fracture F2 rock, the ZPs were −31 and −26 mV in 3 mM and 12 mM solutions, respectively.

Microsphere Properties. The ZP of all of the microspheres varied between −35 to −68 mV in both 3 and 12 mM solutions. The ZP of M-1 (20 nm) decreased with increasing ionic strength (IS); whereas, the ZP of microsphere M-2 (200) and M-3 (500 nm) did not change significantly with increasing IS. The average hydrodynamic diameters (HDs) of the microspheres M-1 and M-2 were larger than the supplier-specified sizes, but the HD of microsphere M-3 was close to the supplier-specified size. The polydispersivity index (PDI) values for M-1 were between 0.27 and 0.33, which indicated the possibility of agglomeration of the particles or presence of particles with a wide size range. In contrast, the PDIs for microspheres M-2 and M-3 were less than 0.08 in all solutions indicating monodispersive particle diameters.[25] Plots containing the ZP and HD results are provided in the Supporting Information.

Bromide Transport. The mass recovery (MR) of bromide was between 95 to 100% in all of the test cases for both fractures. However, significant late stage tailing in the bromide breakthrough curves (BTCs) was consistent with diffusive processes. Bromide could diffuse from the large aperture fracture regions (flowing water regions) to the low aperture fracture regions[26] and to the porous rock matrix near the fracture[1,10,27] (stagnant water regions) due to diffusion. During the flushing phase, the bromide could diffuse back into the flowing water regions and contribute to the high concentration in the BTC tail.[10,26,27] The fitted values for immobile porosity fraction (f) and dispersivity (α_L) were higher for Fracture F1 than for Fracture F2 (see Supporting Information), consistent with the greater aperture variability and matrix porosity of F1.

Effect of Microsphere Size. Figure 1 shows the microsphere breakthrough curves (BTCs) at 3 mM ionic strength (IS) for the three microsphere sizes and three specific discharges for Fractures F1 and F2. The BTC for M-3 was very similar to the BTC for bromide, except for a slightly earlier breakthrough and less tailing at later times. This is attributed to size exclusion for M-3 from the lowest aperture regions,[28] and to diffusion of bromide into and out of the low aperture regions and the pore spaces of the rock matrix.[27] The lack of tailing in the M-3 BTC indicates insignificant matrix and low aperture

dx.doi.org/10.1021/es301721f | Environ. Sci. Technol. 2012, 46, 9987−9994

regions diffusion effects compared to bromide. McKay et al.[7] observed a similar but larger effect in field scale solute and colloid transport experiments in fractured clay, and the effect has also been demonstrated using numerical modeling.[2] Microspheres M-2 showed slightly more retention than M-3, as indicated by peak C/C_o values and MR (Supporting Information). The retention of M-1 was the greatest of the three microspheres tested (Figure 1).

Effect of Specific Discharge. The peak normalized concentration (C/C_o) of the larger microsphere M-3 was not affected by specific discharge (SD) (Figure 1), while the peak C/C_o of microspheres M-1 and M-2 increased with increasing SD. The retention of M-1 was the greatest of the three microspheres tested, and showed the greatest impact of SD on peak C/C_0 values (Figure 1) and mass recovery (MR) as SD increased. The impact of SD on M-1 and M-2 retention in the dolomite fractures is consistent with other studies of SD on colloid retention in fractured shale saprolite[29] and porous media.[30] However, Becker et al.[31] found that breakthrough of 0.28 and 0.98 μm CML microspheres in fractured tuff was not flow rate dependent.

The change in mean residence time (MRT) of microsphere M-1 was not linear for the 12 mM ionic strength (IS) condition in Fracture F1 and for both IS conditions (3 mM and 12 mM) in Fracture F2 (Figure 2). In all other cases, the change in MRT

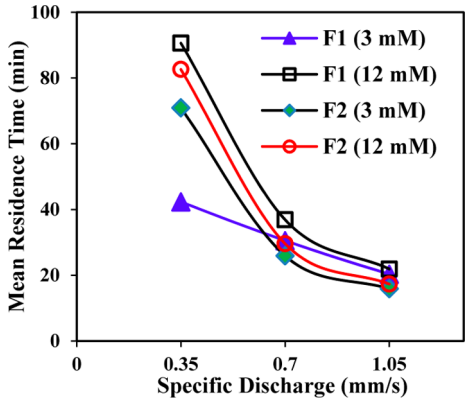


Figure 2. Effects of specific discharge on mean residence time of microsphere M-1.

was linear with the change in SD, as one would expect with simple advective-dispersive transport. This nonlinear effect of SD on the MRT of microsphere M-1 indicates the increasing relative effect of attachment as SD is reduced and IS is increased.

Effect of Ionic Strength. Figure 3 shows the breakthrough curves (BTCs) for 12 mM ionic strength (IS) solutions for the three microspheres with three specific discharge (SD) values for the two fractures tested. Comparing Figure 3 to Figure 1, the increase in ionic strength has a significant effect on the BTCs for M-1 and M-2, and little or no effect for M-3, which has little retention for any condition. As the ZP of the dolomite rock and microspheres became less negative with increases in IS (see Supporting Information), an increase in retention with increasing IS is expected due to electric double layer suppression[32] and this effect has been demonstrated in many experiments in porous media.[9,13,32]

Effects of Aperture Variability. The analysis of fracture aperture indicated much greater aperture variability for F1 compared to F2. In the separate outlet tests, the water flow rates were different for each outlet. For Fracture F1, the flows were 6, 28, 24, 28, and 14% of the total flow in outlets 1, 2, 3, 4, and 5 (see Figure 2S of Supporting Information), respectively. In case of Fracture F2, the corresponding flows were more similar at 18, 18, 20, 19, and 25% of the total flow. The aperture variability effect was also evident in the bromide BTCs (not shown) and the microsphere BTCs (Figure 4). The BTCs for different ports were more distinct for Fracture F1 compared to Fracture F2, and the differences between ports were much greater for the smaller microspheres, with M-1 showing the greatest effect. The bromide BTCs for separate port measurements showed similar trends as M-3, but with later breakthrough and greater tailing due to matrix diffusion effects and/or diffusion into and out of very low aperture regions in the fractures.

Microsphere Transport Parameters. The fitting of the microsphere breakthrough curves (BTCs) with HYDRUS-1D two-site kinetic model resulted in the first type of the sites with a relatively fast attachment coefficient (K_{att1}, 5.0×10^{-5} to 6.0×10^{-3} s^{-1}) and slow detachment coefficient (K_{det1}, 1.0×10^{-6} to 7.0×10^{-5} s^{-1}) for all of the microspheres in both fractures. The second type had fast attachment coefficient (K_{att2}, 2.0×10^{-4} to 3.7×10^{-3} s^{-1}) and fast detachment coefficient (K_{det2}, 2.0×10^{-4} to 4.5×10^{-3} s^{-1}) for all of the microspheres. The R^2 value of the fitting was higher than 94.8% in all the test cases. The first type of site showed a trend of increasing attachment coefficient with increased specific discharge except for M-2 (attachment coefficient decreased from 0.70 $mm \cdot s^{-1}$ specific discharge (SD) case to 1.05 $mm \cdot s^{-1}$ SD case in Fracture F1). The attachment coefficient also decreased with increasing microsphere size. The second type of sites had increased detachment coefficients for increasing SD in both fractures. The first type detachment coefficient (K_{det1}) values were very low; however, they were necessary to fit the low concentrations in the long tails of the BTCs. Although there is no specific experimental evidence for the existence of two types of attachment sites for microspheres, the two-site kinetic model gave a much better match to the experimental results than a one-site kinetic model. The need for a two-site kinetic model to simulate colloid transport in porous media has been previously demonstrated.[33,34]

Mechanisms of Microsphere Retention. The results indicate significant impacts of microsphere size, ionic strength (IS), and fracture characteristics on microsphere transport, with microsphere size being the most significant factor. One might hypothesize that the greater retention of M-1 is due to diffusion of M-1 into low velocity regions associated with small aperture regions and the rock matrix adjacent to the fractures. Bromide transport tests indicated significant effects of diffusion into low velocity regions, with greater effects for F1 compared to F2, consistent with the greater aperture variability and matrix porosity of F1 (Supporting Information). As the diffusion coefficient for M-1 is 2.26×10^{-11} $m^2 \cdot s^{-1}$ compared to 2.1×10^{-9} $m^2 \cdot s^{-1}$ for bromide, the diffusion of M-1 into the low aperture regions and matrix would be much less than bromide diffusion. In the transport tests the retention of M-1 was greater in F2 compared to F1, which would indicate that diffusion into low velocity regions was not the dominant control on retention of M-1 in the dolomite rocks tested. Thus, the greater attenuation of M-1 in F2 is not attributed to porosity or aperture variability differences. This is in contrast to the results of Bales et al.,[10] who attributed apparent retardation of bacteriophages MS2 and f2 to diffusion into shallow pores of

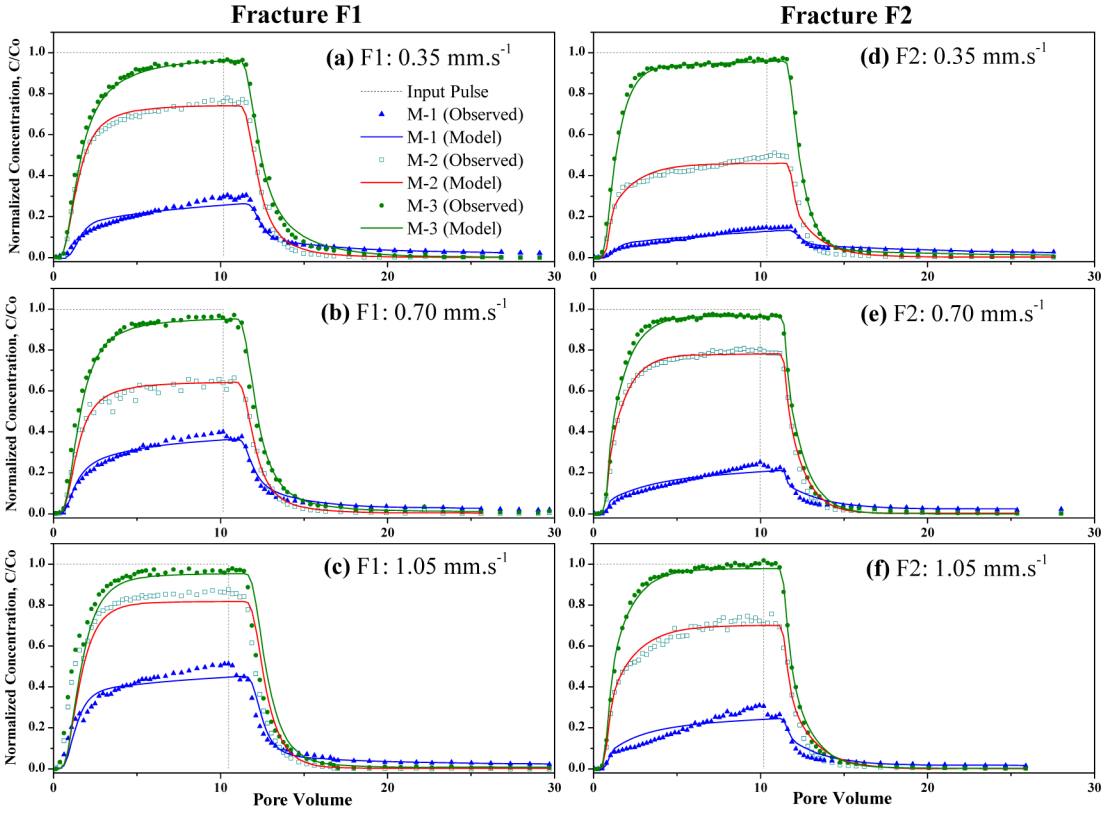


Figure 3. Microsphere BTCs at different specific discharges at Fractures F1 and F2 (ionic strength =12 mM).

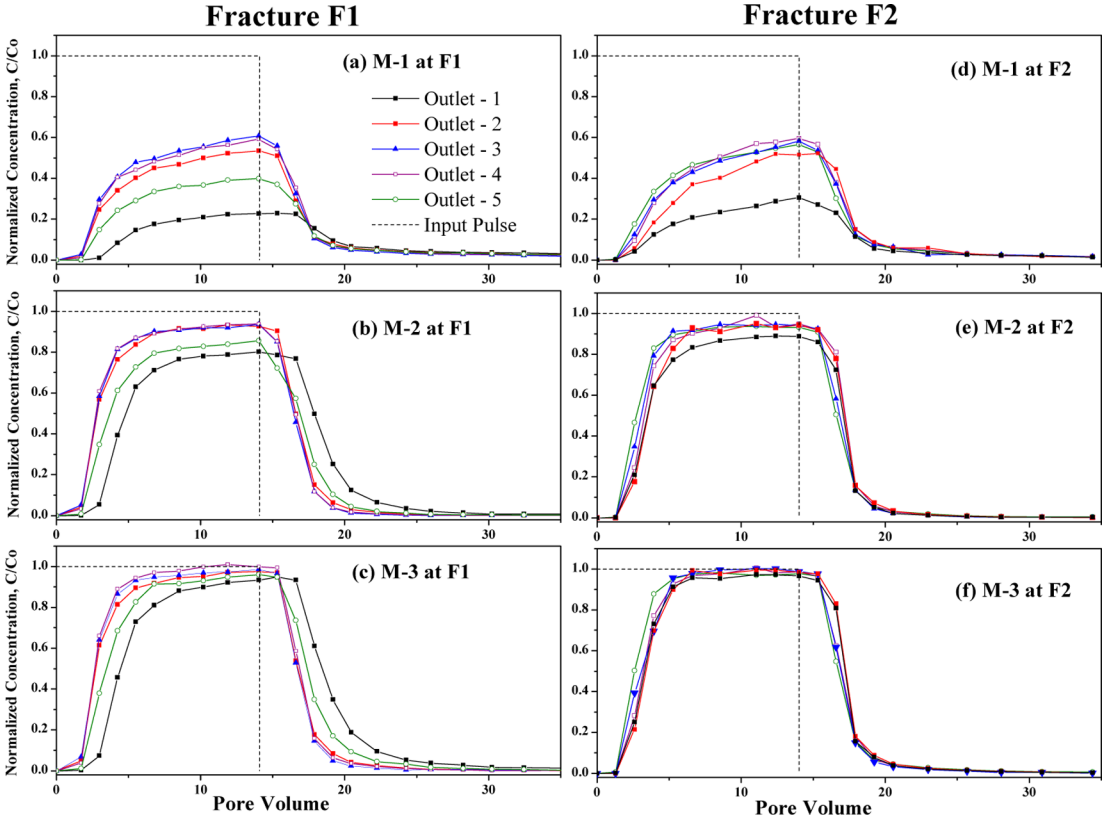


Figure 4. Microsphere BTCs at different outlets at Fractures F1 and F2 (ionic strength = 12 mM, specific discharge = 1.05 mm·s^{-1}).

the matrix of fractured tuff. Cumbie and Mckay[8] attributed apparent retardation of smaller microspheres (0.05 and 0.1 μm) compared to larger microspheres (0.5 and 1 μm) to matrix diffusion in shale saprolite.

dx.doi.org/10.1021/es301721f | Environ. Sci. Technol. 2012, 46, 9987−9994

The overall conditions for attachment of the microspheres to the rock fracture walls was unfavorable, as both microspheres and rock materials had net negative ZP. Retention of colloids in porous media under unfavorable conditions is usually attributed to retention in the secondary energy minimum.[13,14,35] Derjaguin−Landau−Verwey−Overbeek (DLVO) calculations (not shown) indicate that this is possible for the microsphere-rock system of this study. This possibility was further examined by following a 12 mM IS colloid solution injection and flush-out with a subsequent low ionic strength (IS) (1 mM $NaHCO_3$) solution (Figure 5). A significant release of M-1 was observed (~4%). The release of M-2 was 1% and M-3 release was insignificant. This release of M-1 and M-2 by the low IS flush supports the hypothesis that M-1 and M-2 retention was associated with secondary energy minimum effects.[36]

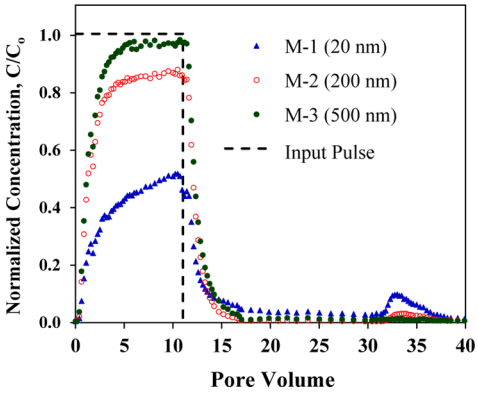


Figure 5. Release of microspheres with low ionic strength solution (Fracture F1; IS = 12 mM; SD = 1.05 mm·s^{-1}).

Increasing IS increases the depth of the secondary energy minima for all microspheres, potentially increasing retention as IS is increased, consistent with results for 3 mM and 12 mM tests (Figures 1 and 3). A secondary minimum energy effect is also consistent with the observation that retention of M-1 was greater in Fracture F2 compared to F1, as F2 had a less negative ZP than F1 at both 3 mM and 12 mM IS.

DLVO calculations indicate that the depth of the secondary energy minimum would increase with increasing microsphere size. Thus, the observed decrease of retention with increasing microsphere size cannot be explained by differences in the magnitude of secondary energy minimum retention. Diffusion plays a significant role with retention in the secondary energy minimum, as demonstrated by the single collector contact efficiency correlation of Tufenkji and Elimelech.[32] The single collector contact efficiency is the probability of colloid collision with the collector surfaces[15] and can be calculated using the equation proposed by Tufenkji and Elimelech.[32] Assuming a collector diameter equal to half of the fracture aperture, and a porosity equal to the volume calculated from the area and hydraulic aperture of the fracture divided by the actual measured fracture volume (gives 0.68 for F1 and 0.87 for F2), and using other parameters based on the experimental conditions, the single collector contact efficiency for M-1 is approximately six times that of the M-2, and 11 times that of M-3. The largest term contributing to the collector contact efficiency is the diffusive term, and therefore the observed impact of microsphere size on retention appears to be directly related to differences in rates of diffusion across streamlines to the fracture walls where retention in the secondary minimum can occur. The attachment coefficient of a particle is proportional to the product of single collector contact efficiency and attachment efficiency (probability of attachment upon collision). Interestingly, the K_{att1} values (Supporting Information) from fitting the two-site kinetic model to the 12 mM data (in Figure 3) for the different microsphere sizes are in similar ratios as the single collector contact efficiencies for the three microsphere sizes.

Hahn and Omelia[37] developed a model to predict the attachment efficiency for retention in the secondary energy minimum. This model predicts that attachment efficiency increases as particle size increases, offsetting the effect of particle size on single collector contact efficiency. The results of the current study would suggest that the effects of particle size on attachment efficiency were less significant than the effects of particle size on rates of particle diffusion to the fracture walls. Surface charge heterogeneity (patches of oppositely charged sites) has also been invoked as having a significant role in the colloid retention under overall unfavorable attachment conditions.[15,16] Bradford et al.[13] suggested that smaller colloids would be affected more by the surface charge heterogeneity as the size approaches that of the heterogeneity on the collector surface. If this phenomenon was influencing results in the current study, then it suggests that the sizes of charge heterogeneities were between 200 and 500 nm. Retention of particles in pits and crevices associated with surface roughness on collector surfaces has also been proposed to contribute to particle retention.[38] Scanning electron microscope (SEM) analysis of the fracture surfaces indicates the presence of substantial roughness that could trap colloids, and this trapping could be more favorable to smaller microspheres due to higher rates of diffusion into the pits and crevices, and due to size exclusion effects associated with small aperture regions for the larger microspheres. However, F1 was rougher than F2, yet higher retention of M-1 was observed in F2 compared to F1.

The greater retention of M-1 in F2 compared to F1 may be related to the smaller aperture of F2. With the smaller aperture of F2, the distance for diffusion to the fracture walls would be less than for F1, resulting in a higher rate of microspheres reaching the walls in F2 where they could be retained in the secondary minimum, in positively charged areas, or in surface roughness. The less negative ZP of F2 could also result in greater retention of particles in secondary minima as the depth of the secondary energy minimum would be greater for the less negative ZP of F2. As the factors of ZP and aperture are confounded in this study, it is not possible to determine which one was more dominant in producing the greater retention of M-1 in F2. However, the tests with different IS show that the retention is very sensitive to IS, which would affect ZP, suggesting that a difference in ZP between the fractures would be expected to have an effect on retention of M-1.

IMPLICATIONS

Fracture aperture variability, matrix porosity, mineral composition, solution ionic strength, specific discharge, and colloid size will significantly affect colloid transport behavior in fractured dolomite. Values of pH in dolomite rock would be expected to be at or above 8, for which the overall fracture surface charge would be negative. On the basis of this study, negatively charged colloids on the order of 500 nm diameter would be expected to be mobile in dolomite rock with hydraulic apertures as low as 95 μm due to the unfavorable

attachment conditions and limited attachment in secondary energy minima due to the low colloid diffusion coefficients. In contrast, as colloid size is decreased to as low as 20 nm, increasing retention would be expected, likely due to retention in the secondary energy minimum, and perhaps surface charge heterogeneity and surface roughness effects. The reversibility of retention in secondary energy minima, demonstrated in this study, indicates that colloidal particles retained in fractured dolomite may be remobilized by changes in groundwater chemistry. Thus, the prediction of colloid mobility in fractured dolomite requires extensive characterization of rock and colloid properties. While matrix diffusion may have a significant impact on solute transport in dolomite rock, the impact on microsphere transport appears to be minor, even for the 20 nm microspheres. Model fitting indicates that a two-site kinetic model is required to predict colloid movement in fractures at the bench scale, with parameters being sensitive to physical and chemical properties of colloids and rock, as well as flow rates. The extrapolation of bench scale models to field scale predictions will require development of scale-up procedures from numerical modeling and comparison of bench and field scale tests for similar rock properties.

■ ASSOCIATED CONTENT

Supporting Information

Additional information regarding materials and methods used, experimental system and configuration, and results. This material is available free of charge via the Internet at http://pubs.acs.org.

■ AUTHOR INFORMATION

Corresponding Author

*Phone: (416) 978-3005; fax: (416) 978-6813; e-mail: brent.sleep@utoronto.ca.

Notes

The authors declare no competing financial interest.

■ ACKNOWLEDGMENTS

This research was supported by the Canadian Water Network (CWN) through the Pathogens-in-Groundwater Research Consortium and the Natural Sciences and Engineering Research Council of Canada (NSERC) Discovery Grant of Sleep.

■ REFERENCES

(1) Abdel-Salam, A.; Chrysikopoulos, C. V. Modeling of colloid and colloid-facilitated contaminant transport in a two-dimensional fracture with spatially variable aperture. *Transp. Porous Media* **1995**, *20*, 197−221.

(2) James, S. C.; Chrysikopoulos, C. V. Transport of polydisperse colloids in a saturated fracture with spatially variable-aperture. *Water Resour. Res.* **2000**, *36* (3), 1457−1465.

(3) Reimus, P. W. The use of colloids in tracer transport experiments in saturated rock fractures, Report LA-13004-T. Los Alamos National Laboratory: Los-Alamos, NM, 1995.

(4) Becker, M. W.; Metge, D. W.; Collins, S. A.; Shapiro, A. M.; Harvey, R. W. Bacterial transport experiments in fractured crystalline bedrock. *Ground Water* **2003**, *41*, 682−689.

(5) Champ, D. R.; Schroeter, J. Bacteria transport in fractured rock-a field scale tracer test at the Chalk River nuclear laboratories. *Water Sci. Technol.* **1988**, *20* (11−12), 81−87.

(6) Frazier, C. S.; Graham, R. C.; Shouse, P. J.; Yates, M. V.; Anderson, M. A. A field study of water flow and virus transport in weathered granitic bedrock. *Vadose Zone J.* **2002**, *1*, 113−124.

(7) McKay, L. D.; Gillham, R. W.; Cherry, J. A. field experiments in a fractured clay till: 2. Solute and colloid transport. *Water Resour. Res.* **1993**, *29* (12), 3879−3890.

(8) Cumbie, D. H.; McKay, L. D. Influence of diameter on particle transport in a fracture shale saprolite. *J. Contam. Hydrol.* **1999**, *37*, 139−157.

(9) McCarthy, J. F.; McKay, L. D.; Burner, D. D. Influence of ionic strength and cation charge on transport of colloidal particles in fractured shale saprolite. *Environ. Sci. Technol.* **2002**, *36*, 3735−3743.

(10) Bales, R.; Gebra, C.; Grondin, G.; Jensen, S. Bacteriophage transport in sandy soil and fractured Tuff. *Appl. Environ. Microbiol.* **1989**, *55*, 2061−2067.

(11) Grindrod, P. The impact of colloids on the migration and dispersal of radionuclides within fractured rock. *J. Contam. Hydrol.* **1993**, *13*, 167−181.

(12) McKay, L. D.; Cherry, J. A.; Bales, R. C.; Yahya, M. T.; Gerba, C. P. A field example of bacteriophage as tracers of fracture flow. *Environ. Sci. Technol.* **1993**, *27*, 1075−1079.

(13) Bradford, S. A.; Torkzaban, S.; Šimůnek, J. Modeling colloid transport and retention in saturated porous media under unfavorable attachment conditions. *Water Resour. Res.* **2011**, *47*, W10503 DOI: 10.1029/2011WR010812.

(14) Kuznar, Z. A.; Elimelech, M. Adhesion kinetics of viable *Cryptosporidium parvum* oocysts to quartz surfaces. *Environ. Sci. Technol.* **2004**, *38*, 6839−6845.

(15) Johnson, W. P.; Tong, M. Observed and simulated fluid drag effects on colloid deposition in the presence of an energy barrier in an impinging jet system. *Environ. Sci. Technol.* **2006**, *40*, 5051−5021.

(16) Ryan, J. N.; Elimelech, M. Colloid mobilization and transport in groundwater. *Colloids Surf., A* **1996**, *107*, 1−56.

(17) Chrysikopoulos, C. V.; Masciopinto, C.; La Mantia, R.; Manariotis, I. D. Removal of biocolloids suspended in reclaimed wastewater by injection in a fractured aquifer model. *Environ. Sci. Technol.* **2010**, *44* (3), 971−977.

(18) Masciopinto, C.; La Mantia, R.; Chrysikopoulos, C. V. Fate and transport of pathogens in a fractured aquifer in the Salento area, Italy. *Water Resour. Res.* **2008**, *44*, W01404 DOI: 10.1029/ 2006WR005643.

(19) Reitsma, S. Laboratory Measurement of Capillary Pressure-saturation Relationships in Natural Rock Fractures. M.A.Sc. Thesis, Department of Earth Sciences, University of Waterloo: Ontario, Canada, 1992.

(20) Šimůnek, J.; Šejna, M.; Saito, H.; Sakai, M.; van Genuchten, M. Th. The HYDRUS-1D software package for simulating the one-dimensional movement of water, heat, and multiple solutes in variably-saturated media, version 4.0, *HYDRUS Software Series 3*, Department of Environmental Sciences, University of California—Riverside: Riverside, California, U.S.A., 2008.

(21) Grasselli, G.; Wirth, J.; Egger, P. Quantitative three-dimensional description of a rough surface and parameter evolution with shearing. *Int. J. Rock Mech. Min. Sci.* **2002**, *39*, 789−800.

(22) Gence, N.; Ozbay, N. pH dependence of electrokinetic behavior of dolomite and magnesite in aqueous electrolyte solutions. *Appl. Surf. Sci.* **2006**, *252*, 8057−8061.

(23) Malysiak, V.; O'Connor, C. T.; Ralston, J.; Gerson, A. R.; Coetzer, L. P.; Bradshaw, D. J. Pentlandite−feldspar interaction and its effect on separation by flotation. *Int. J. Miner. Process.* **2002**, *66*, 89−106.

(24) Parks, G. A. The isoelectric points of solid oxides, solid hydroxides, and aqueous hydroxo complex systems. *Chem. Rev.* **1965**, *65* (2), 177−198, DOI: 10.1021/cr60234a002.

(25) Nobbmann, U.; Connah, M.; Fish, B.; Varley, P.; Gee, C.; Mulot, S.; Chen, J.; Zhou, L.; Lu, Y.; Sheng, F.; Yi, J.; Harding, S. E. Dynamic light scattering as a relative tool for assessing the molecular integrity and stability of monoclonal antibodies. *Biotechnol. Genet. Eng. Rev.* **2007**, *24*, 117−128.

(26) Neretnieks, I. A note on fracture flow dispersion mechanisms in the ground. *Water Resour. Res.* **1983**, *19* (2), 364−370.

(27) Reimus, P. W.; Callahan, T. J. Matrix diffusion rates in fractured volcanic rocks at the Nevada Test Site: Evidence for a dominant

influence of effective fracture apertures. *Water Resour. Res.* **2007**, *43*, W07421 DOI: 10.1029/2006WR005746.
(28) Chrysikopoulos, C. V.; Abdel-Salam, A. Modeling of colloid transport and deposition in saturated fractures. *Colloids Surf., A* **1997**, *121*, 189−202.
(29) Mckay, L. D.; Harton, A. D.; Wilson, G. V. Influence of flow rate on transport of bacteriophage in shale saprolite. *J. Environ. Qual.* **2002**, *31*, 1095−1105.
(30) Tong, M.; Johnson, W. P. Excess colloid retention in porous media as a function of colloid size, fluid velocity, and grain angularity. *Environ. Sci. Technol.* **2006**, *40* (24), 7725−7731, DOI: 10.1021/es061201r.
(31) Becker, M. W.; Reimus, P. W.; Vilks, P. Transport and attenuation of carboxylate-modified latex microspheres in fractured rock laboratory and field tracer tests. *Ground Water* **1999**, *37* (3), 387−395.
(32) Tufenkji, N.; Elimelech, M. Breakdown of colloid filtration theory: Role of the secondary energy minimum and surface charge heterogeneities. *Langmuir* **2005**, *21*, 841−852.
(33) Schijven, J. F.; Hassanizadeh, S. M.; de Bruin, R. H. A. M. Two-site kinetic modeling of bacteriophages transport through columns of saturated dune sand. *J. Contam. Hydrol.* **2002**, *57*, 259−279.
(34) Schijven, J. F.; Hassanizadeh, S. M. Removal of viruses by soil passage: Overview of modeling, processes, and parameters. *Crit. Rev. Environ. Sci. Technol.* **2000**, *30* (1), 49−127.
(35) Litton, G. M.; Olson, T. M. Particle size effects on colloid deposition kinetics: Evidence of secondary minimum deposition. *Colloids Surf., A* **1996**, *107*, 273−283.
(36) Franchi, A.; O'Melia, C. R. Effects of natural organic matter and solution chemistry on the deposition and reentrainment of colloids in porous media. *Environ. Sci. Technol.* **2003**, *37*, 1122−1129.
(37) Hahn, M. W.; O'Melia, C. R. Deposition and reentrainment of Brownian particles in porous media under unfavorable chemical conditions: Some concepts and applications. *Environ. Sci. Technol.* **2004**, *38*, 210−220.
(38) Gregory, J.; Wishart, A. J. Deposition of latex-particles on alumina fibers. *Colloids Surf.* **1980**, *1*, 313−334.